Endothermic effects in porous silica doped with silver nanoparticles and the formation of Ag_2O by atmospheric oxygen via chemisorption

1997 J. Phys.: Condens. Matter 9 1995

(http://iopscience.iop.org/0953-8984/9/9/013)

J. Phys.: Condens. Matter **9** (1997) 1995–2008. Printed in the UK PII: S0953-8984(97)74482-5

Endothermic effects in porous silica doped with silver nanoparticles and the formation of Ag_2O by atmospheric oxygen via chemisorption

Cai Weiping, Tan Ming and Zhang Lide

Institute of Solid State Physics, Academia Sinica, Hefei 230031, Anhui, People's Republic of China

Received 14 May 1996, in final form 22 October 1996

Abstract. Porous silica dispersed with silver (Ag) nanoparticles (about 3 nm in diameter) within its pores has been prepared by a new method. The microstructures and the size distribution of particles within pores have been examined by transmission electron microscopy and the Brunauer–Emmett–Teller technique. The Ag nanoparticles are uniformly dispersed within the pores of silica; the particle size follows the log-normal distribution function. The thermal effect of this porous composite, exposed to ambient air for different times, has been investigated by differential scanning calorimetry and thermogravimetric analysis. An endothermic peak has been found for all the doped samples measured. At room temperature (298 K), a short exposure (2 d) to dry air leads to a wide endothermic peak at around 400 K; long exposure (1 month) results in a wider endothermic peak at around 450 K; when the sample was exposed to ambient air with relative humidity greater than 60%, a much higher endothermic peak exists at around 460 K. From the experimental results and discussions of adsorption and oxidation, the endothermic peaks for the samples exposed to dry air can be mainly attributed to the desorption of oxygen physisorbed and chemisorbed on the surface of the Ag particles within the pores, for lower- and higher-temperature peaks, respectively, and the corresponding desorption enthalpy values were estimated to be about 0.26 eV and 0.90 eV, respectively. For the sample exposed to humid air, the endothermic peak originates from the decomposition of silver oxide (Ag_2O) formed on the surface layer of the Ag particles, and the bond energy of Ag–O in the Ag_2O film was estimated to be about 1.8 eV.

1. Introduction

Porous solids with mesoscopic pores and a high specific surface area, doped with the nanosized particles (metals, semiconductors or compounds), display many unique properties and have received considerable attention in recent years [1–4]. For example, a dispersion of semiconductor ultrafine particles within the pores of porous glass leads to optical switching and optical non-linearity [5]. Porous glass doped with silver (Ag) nanoparticles in its pores by a wet chemical reaction method displays a novel electrical switching and memory effect in different ambient gases [6, 7] and can be used as gas-detecting elements. Because all the pores in porous solids are interconnected and open to the ambient air, the particles within the pores are also in contact with the ambient air. Because the particles are small in size and chemically active [8, 9], we suggest that there certainly exists interactions between the ambient air and the particles within the pores. Therefore adsorption, desorption or even chemical reaction on the surface of the particles could occur in the different ambient conditions and hence cause variation in the properties (including optical absorption) of

0953-8984/97/091995+14$19.50

particle-doped porous solids. On the basis of these ideas, recently we have synthesized a new material by putting Ag nanoparticles into the pores of porous silica with a high specific surface area, with the help of the sol–gel technique and the thermal decomposition of silver nitrate ($AgNO_3$). This material assumes an optical switching and memory effect in different ambient conditions; this will be reported in another paper. Here we investigate the thermal stability of this material, Ag-nanoparticle-doped porous silica, after exposure to the ambient air for different times. First we present the preparation method of this material.

2. Experiments

The monolithic porous silica was prepared from tetraethyl orthosilicate, alcohol, distilled water and a small amount of nitric acid by the sol–gel technique [10, 11], followed by thorough cleaning (to pH 7) with distilled water, drying at a temperature from 298 to 423 K and finally annealing at 873 K for 2 h. The final porosity is estimated to be 50% by the pycnometry technique. The pre-formed monolithic porous silica was then soaked in the 0.25 M $AgNO_3$ solution at room temperature (298 K). After it had been soaked in the solution for a sufficiently long time (more than 3 weeks), the sample was taken out and dried at a temperature from 298 to 423 K to remove the solvent from it and to retain the $AgNO_3$ microcrystals in the pores. Then the dried sample was heated in the air to 623 K and held for 2 h to let the remaining $AgNO_3$ decompose [12], leaving silver particles only within the pores of the silica. The undoped sample was also subjected to the same additional heat treatment for reference.

The heat-treated monolithic doped sample was ground. The powders obtained in this way were dispersed in acetone in a test-tube. The latter was placed in an ultrasonic bath for 10 min. The clear liquid from the top portion of the test tube was taken and a few drops of this liquid were placed on a carbon-coated copper grid. After evaporation of the acetone the copper grid was mounted in a JEM 200 CX transmission electron microscope operated at 200 kV; hence the microstructure and selected-area electron diffraction pattern were investigated, and the size and distribution of microcrystals were inspected.

After heat treatment at 623 K for 2 h, the porosity, density and specific surface area for the undoped and doped samples were measured by pycnometry and the Brunauer–Emmett–Teller (BET) technique using N_2 gas in an ASAP2000 instrument, made by Micromerics. Differential scanning calorimetry (DSC) measurements were conducted in argon with a Perkin–Elmer DSC-2 differential scanning calorimeter. The thermogravimetry (TG) measurements were performed in argon using a Shimadzu DT-50 thermal analysis system. For the doped and undoped samples after heat treatment at 623 K for 2 h, the subsequent treatments before DSC or TG measurements are listed in table 1. The DSC or

Table 1. Treatments of the heat-treated reference and doped sample before DSC of TG measurements.

Sample	Type of sample (623 K for 2 h)	Treatment (298 K)
0	Reference	Exposure to dry air for 7 d
1	Doped	Exposure to dry air for 2 d
2	Doped	Exposure to dry air for 30 d
3	Doped	Exposure for 7 d to wet air with relative humidity greater than 60%

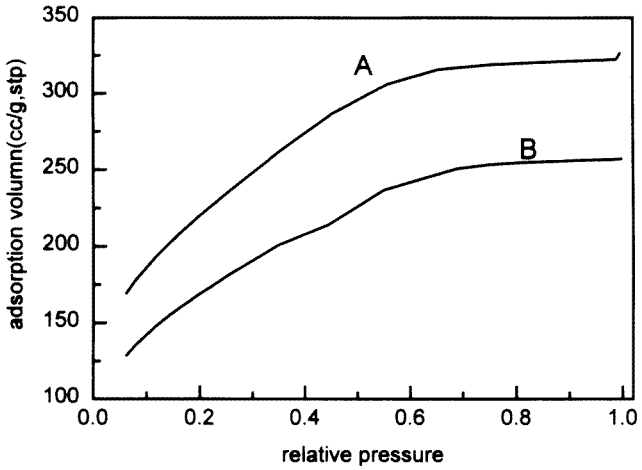

Figure 1. Nitrogen sorption isotherms of the undoped sample (reference) (curve A) and the doped sample after heat treatment at 623 K for 2 h (curve B) for 2 h.

TG measurements start from 330 to 573 K and the corresponding curves were obtained at a scanning rate of 10 K min^{-1}. For DSC measurements, the second run for each sample was conducted *in situ* immediately after finishing the first run (heating from 330 to 573 K and then cooling to 330 K), and all the curves for the second run are parallel to the temperature axis (no peak was observed).

3. Results

3.1. Characterization

The amount of silver dopant in the porous silica is estimated to be about 10 wt% from the density data of the doped sample and the undoped reference sample. The specific surface area decreases significantly from 760 m^2 g^{-1} for the reference sample to 460 m^2 g^{-1} for the doped sample. This is attributed to the presence of the particles within the pores of the silica, which is shown more clearly by the N_2 isothermal adsorption curves for the two samples (figure 1). The whole curve for the doped sample is obviously lower than that of the reference sample. The slope for the former is less than that of the latter in the relative pressure range 0.05–0.7 which corresponds to pores with mesoscopic curvature radius. This means that particles exist within the mesoscopic pores.

Figure 2(a) is a transmission electron micrograph of the doped sample, the particles being uniformly dispersed. Figure 2(b) is a selected-area electron diffraction pattern from the micrograph shown in figure 2(a). The values of interplanar spacings have been calculated from the diameters of these rings in figure 2(b) and are given in table 2. The standard ASTM d_{hkl} values for silver are also shown in this table. The observed data agree with those of the bulk silver. No other crystallites (including $AgNO_3$) were found from our transmission electron microscopy examination. Therefore it is reasonable to suggest that the crystallites within the mesoscopic pores of the porous silica are only (or mainly) Ag particles.

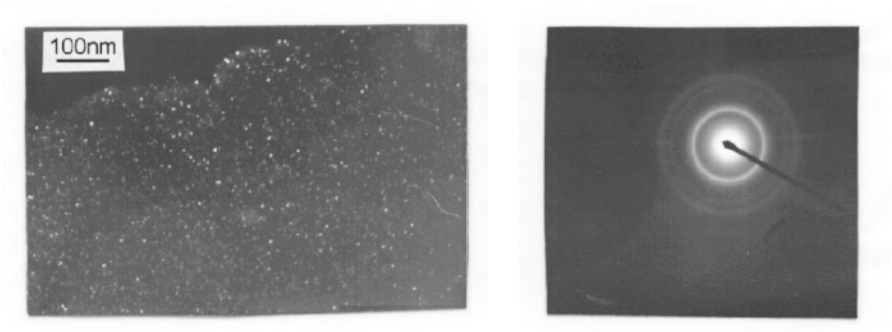

(a) (b)

Figure 2. (a) Electron micrograph of the doped sample after heat treatment at 623 K for 2 h; (b) electron diffraction pattern of (a).

Table 2. Comparison of d_{hkl} values with ASTM data for silver nanoparticles doped in the porous silica.

Observed d_{hkl} (nm)	Standard d_{hkl} for Ag (nm)
0.2398	0.2359
0.2085	0.2043
0.1468	0.1445
0.1249	0.1231
0.0943	0.0938

A histogram of the silver particle sizes is shown in figure 3. It is well fitted with the log-normal distribution function given by

$$\Delta n = \frac{1}{\sqrt{2\pi}\ln\sigma}\exp\left\{-\frac{1}{2}\left[\frac{\ln(d/\bar{d})}{\ln\sigma}\right]^2\right\}\Delta(\ln d) \tag{1}$$

where Δn is the fractional number of particles per logarithmic diameter interval $\Delta(\ln d)$, $\bar{d}$ is the average diameter and σ is the geometric standard deviation. The fitting curve of the midinterval point of histogram is in good agreement with the histogram, as shown in figure 3. The average particle diameter and standard deviation σ-values obtained by the statistical method [13] and fitting according to the log-normal distribution function (equation (1)) are seen in table 3.

Table 3. The average diameter $\bar{d}$ and standard deviation σ of silver particles within pores of silica.

Method	$\bar{d}$ (nm)	σ (nm)
Log-normal	2.4	1.4
Statistic method	2.6	1.1

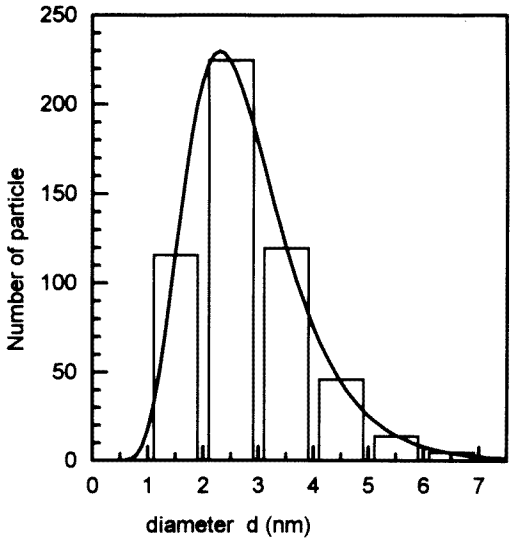

Figure 3. Size distribution histogram of the silver particles in the doped porous silica shown in figure 2(a); the curve is the corresponding fitting result of the midinterval point of histogram by the log-normal function.

3.2. Differential scanning calorimetry measurements

Figure 4 shows the DSC curves for the reference and doped samples after exposure to dry air at room temperature (298 K) for different times (samples 0, 1 and 2). There is no peak for the reference sample (1 week exposure), only a slightly increasing background with increasing measuring temperature. For the doped samples, there is an endothermic peak but the peak temperature and the area under the peak, which corresponds to the process enthalpy, are different for different exposure times in dry air. The doped sample with a 1 month exposure has a higher peak temperature and larger enthalpy change than that with a 2 d long exposure. The peak temperature T_p and the enthalpy values ΔH are listed in table 4. Curve (a) in figure 5 indicates the DSC curve for the doped sample with exposure to the air with relative humidity greater than 60% at 298 K for 1 week (sample 3.1). There exists a very high endothermic peak at around 456 K. In order to eliminate the adsorbed water in the sample during the exposure to the ambient air, the DSC measurement for a similar sample to sample 3.1 was performed after it was heated *in situ* at 378 K for 1 h and cooled to 330 K in the chamber of the DSC system (sample 3.2). The corresponding result is shown as curve (b) in figure 5. We can see that the endothermic peak is much narrower (sharper) than the former. The T_p and ΔH data are also listed in table 4. T_p is close to that of sample 2, but the ΔH-value is much higher, five to 13 times more than for samples 1 and 2.

4. Discussions

On the basis that the adsorption of water (H_2O) in porous silica occurs easily, we design an experiment to investigate the possibility that the endothermic peak for sample 1 is caused by the desorption of H_2O. An undoped sample and a doped sample, which were heat treated

Table 4. Data from DSC measurements on reference and doped samples. T_p is the peak temperature, ΔT is the temperature range of the peak, and ΔH is the enthalpy. Sample 3.1 is sample 3 in table 1 and sample 3.2 is sample 3 with additional *in-situ* heating at 378 K for 1 h and cooling to 330 K before before DSC measurement.

Sample	T_p (K)	ΔT (K)	ΔH (J g^{-1})
0	—	—	—
1	400	345–460	15
2	450	384–540	48
3.1	456	355–524	240
3.2	460	386–524	198

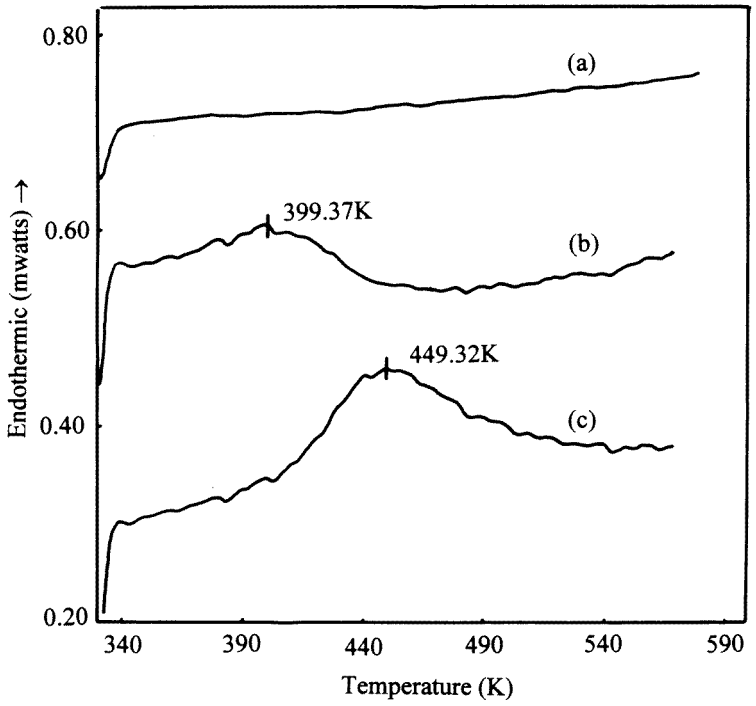

Figure 4. DSC curves for heat-treated samples exposed to dry air (at 298 K): curve (a), undoped sample, exposure for 7 d; curve (b), doped sample, exposure for 2 d; curve (c), doped sample, exposure for 30 d.

at 623 K for 2 h and then exposed to the ambient air (not in a dry jar) at 298 K for 2 d, were measured from 330 to 573 K using the DSC system. The curves are given in figure 6. For the undoped silica, there is an endothermic peak at around 378 K which should be attributed to the desorption of the adsorbed H_2O on the pore wall. For the doped sample, there are two endothermic peaks which partially overlap. The temperature for the lower-temperature peak is in agreement with the peak for the undoped sample (see curves (a) and (b) in figure 6). The undoped and doped samples which had undergone the same treatment were also measured after they had been heated *in situ* at 378 K for 30 min and cooled to

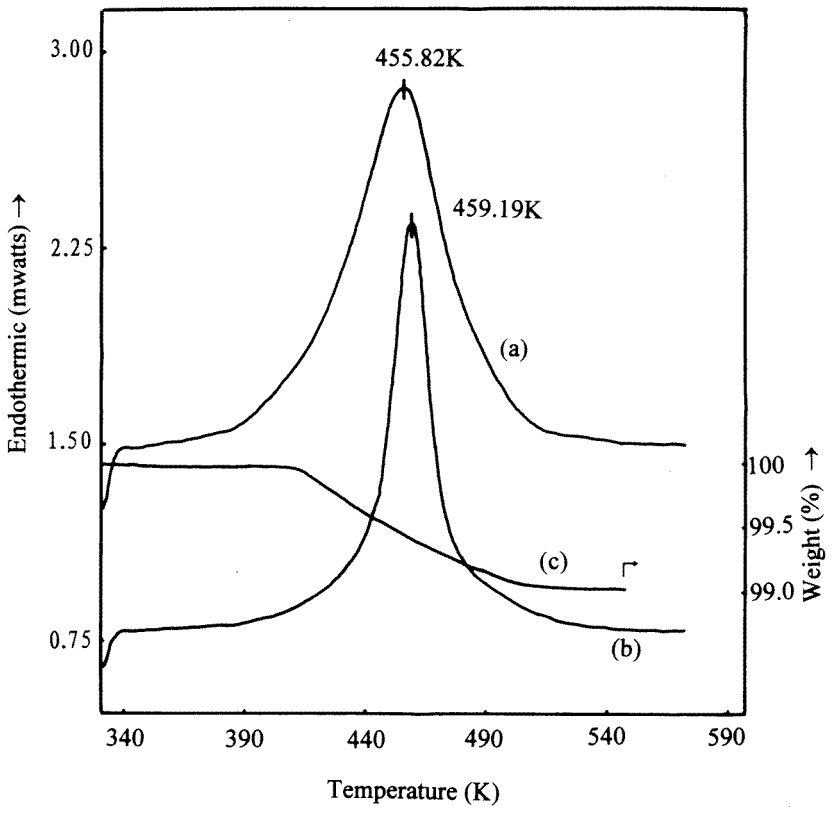

Figure 5. DSC and TG curves for the heat-treated doped sample exposed to ambient air with relative humidity greater than 60% (at 298 K) for 7 d: curve (a), without *in situ* heating before DSC measurement; curve (b), *in situ* heating at 378 K for 1 h before DSC measurement; curve (c), TG curve corresponding to curve (b).

330 K. The peak at around 378 K for both samples disappears, and the two DSC curves are the same as curves (a) and (b) respectively in figure 4. Therefore, the lower-temperature peak (at around 400 K) in figure 4 is not related to the desorption of adsorbed H_2O on the pore wall. Similarly, the peak of curve (c) in figure 4 and the peak of curve (b) in figure 5 should not be mainly attributed to the desorption of H_2O, i.e. adsorbed water can be ignored for the samples exposed to dry air.

It is known, from a previous section of this paper, that there exist a large number of silver nanoparticles within the pores of the porous silica. The pores in silica are interconnected and open to the ambient air; hence the particles within the pores are also in contact with the air. Therefore, oxygen in the air will be adsorbed on the surface of the Ag particles, thereby reducing the energy at room temperature because a free surface with a broken bond possesses a higher energy. Adsorption can be theoretically divided into physical adsorption and chemical adsorption. The physical adsorption originates from the rather weak van der Waals forces. This type of bond involves no charge transfer between the surface atoms and adsorbed molecules. In the case of chemical adsorption, on the other hand, electron exchanges occur between the surface atoms and the adsorbed atoms as in the

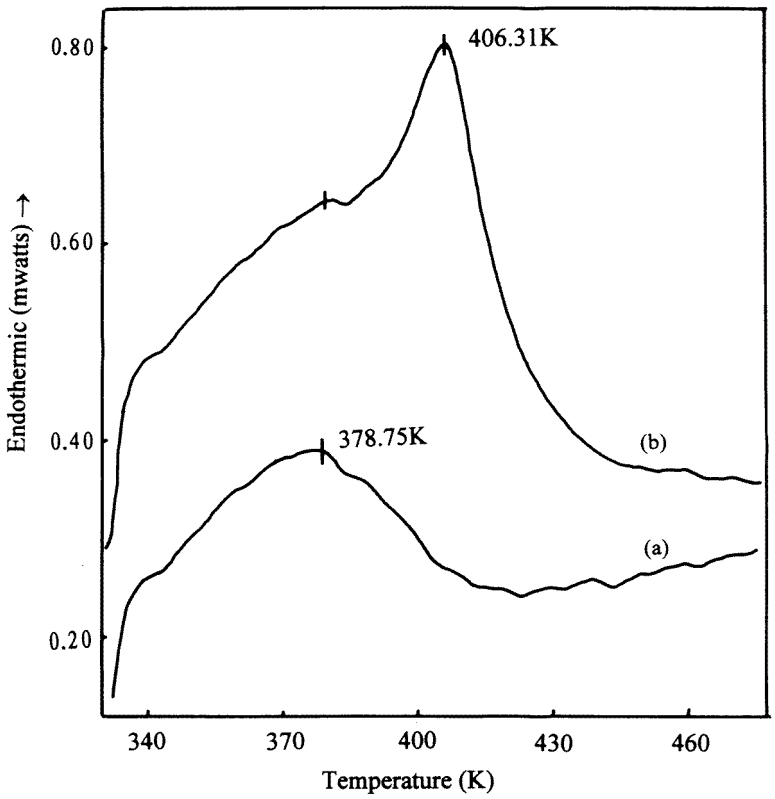

Figure 6. DSC curves for heat-treated samples exposed to ambient air (at 298 K) for 2 d: curve (a), undoped sample (reference); curve (b), doped sample.

case of chemical compounds. The binding energies for physisorbed molecules are typically 0.25 eV or less while the range of binding energies in chemisorption is quite large, ranging from 0.43 to 8.4 eV [14]. When the temperature rises, adsorbed atoms or molecules can receive sufficient energy, which is larger than the binding energy (plus the energy barrier when in chemisorption), from thermal fluctuation to leave the surface or to desorb [14]. This is an endothermic process. Desorption of chemisorbed atoms or molecules will take place at higher temperatures, accompanied by a larger endothermic effect than that of physisorbed atoms or molecules.

4.1. The origins of the endothermic peaks

Here we suggest that the peak for sample 1 (see curve (b) in figure 4) is mainly associated with desorption of the molecules physisorbed on the surface of the Ag particles within pores during a short exposure to dry air.

According to the data on the amount of Ag dopant in silica (10 wt%) and Ag density (10.5 g cm^3), we know that there is about 0.01 cm^3 volume of the silver crystallites in 1 g of the doped sample and there are about 1.2×10^{18} Ag particles if we take the average diameter of the particles as 2.5 nm (see table 3). So the total surface area S of the Ag

particles in 1 g of the doped sample can be obtained from the following equation:

$$S = \int_0^\infty 4\pi \left(\frac{x}{2}\right)^2 N f(x)\,\mathrm{d}x = \pi N \overline{x^2} = \pi N(\sigma^2 + \overline{x^2}) \tag{2}$$

where $N = 1.2 \times 10^{18}$, $f(x)$ is the size distribution function or given by equation (1) and x is the diameter. According to the data listed in table 3, we have the total surface area of Ag particles, which is about 29.5 m^2 in 1 g of the doped sample. Furthermore, from the lattice parameter of silver and the total surface area of Ag particles, we can get the total number of surface atoms of the Ag particles in 1 g of the sample by letting the surface atomic distance be approximately equal to the bulk atomic distance, which is about 3.54×10^{20} surface Ag atoms in 1 g of the sample. Finally, assuming monolayer surface adsorption, we have the desorption enthalpy of the adsorbed molecules, or approximately the binding energy between Ag atoms and adsorbed molecules (ignoring the difference between enthalpy and internal energy). It can be approximately determined by the ratio $\Delta H/(3.54 \times 10^{20})$. For the peak of sample 1, the desorption enthalpy or binding energy is about 0.26 eV. In addition, the physisorption is usually multilayer molecular adsorption. So the real binding energy between the adsorbed molecule and Ag atom should be smaller than 0.26 eV. Therefore, it is justified that the endothermic peak for sample 1 is mainly attributed to the desorption of physisorbed molecules on the surface of the Ag nanoparticles within the pores of silica. Considering that the desorption leads not only to the endothermic effect but also to weight loss, the TG measurement was performed for sample 1, as shown in figure 7. The weight loss in the corresponding temperature range is about 0.42 wt%.

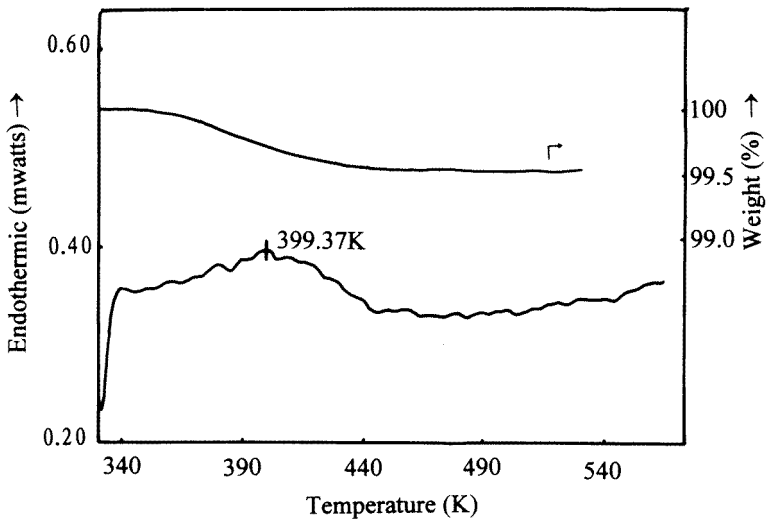

Figure 7. TG and DSC curves for the doped sample exposed to dry air (at 298 K) for 2 d (sample 1).

According to the potential energy curves for physisorption and chemisorption [15], the physisorbent process needs no activation energy and hence occurs easily, and desorption occurs at a lower temperature. This can explain the facts that the adsorption in sample 1 occurs during a short exposure to the air, and the desorption occurs at a lower temperature than for the other samples.

Chemisorption, however need extra energy or activation energy. It has been indicated that the chemisorption usually occurs at some active sites on the surface by the diffusion of physisorbed molecules or atoms [14]. Therefore, the chemisorption usually occurs at a higher temperature than the physisorption process. Our experiments also confirmed this conclusion. During short exposure to the dry air, only physisorption occurs (sample 1). Long exposure to the air leads to chemisorption, and its desorption temperature is also higher (see curve (c) in figure 4). With the help of the calculation of the desorption enthalpy (or binding energy) by the same method as mentioned above for sample 2, we get the value 0.90 eV, which falls into the range of binding energies in chemisorption. TG measurement also proved the existence of weight loss in the corresponding temperature region. Therefore, it is reasonable to suggest that the endothermic peak of sample 2 is mainly caused by the desorption of the molecules chemisorbed on the surface of the Ag particles within the pores.

4.2. Species of the adsorbed molecules

According to the experiments and discussions above, we know that the endothermic peaks for samples 1 and 2 are mainly not associated with the desorption of the adsorbed water. At room temperature, the adsorption of N_2 in the air on the pore wall can be ignored. According to Kilty and Sachtler [16], the O_2 in contact with silver can undergo the two following reactions:

$$\begin{aligned} &O_2 + Ag \rightarrow O_2(ads) + Ag^+ \\ &O_2 + 4Ag \rightarrow 2O^{2-}(ads) + 4Ag^+ \end{aligned} \tag{3}$$

i.e. chemisorption may occur when oxygen is in contact with silver. From these, we suggest that the species of the molecules adsorbed on the surface of the Ag nanoparticles is probably mainly oxygen in the air. The oxygen molecules are adsorbed on the surface of the Ag particles during exposure of the samples to dry air, and first physisorption occurs and then adsorption transforms into chemisorption.

4.3. Surface oxidation of Ag particles

It has been shown that the adsorption of oxygen molecules on the surface of metals will reduce the force constant of oxygen molecules significantly [17]. According to the structural chemistry, the decrease in the force constant of the oxygen molecules adsorbed on the metal means that the O–O bond weakens, or the oxygen molecules adsorbed on the metal are active and hence easily react with the metal.

Thermodynamically, silver may form silver oxide (Ag_2O) with oxygen at room temperature, or the reaction

$$2Ag + \tfrac{1}{2}O_2 \rightarrow Ag_2O \tag{4}$$

may occur, because of the negative standard formation free energy value [18], ($\Delta G_{298} = -11.25$ KJ mol^{-1}) of Ag_2O at room temperature. From equation (4), we have the equilibrium constant K_p [19]:

$$K_P = \frac{a_P}{a_{Ag}^2 P_{O_2}^{1/2}} \tag{5}$$

where a_P and a_{Ag} are the activities of Ag_2O and Ag, respectively; both values are unity. P_{O_2} is the equilibrium partial pressure of oxygen. So we have

$$\Delta G_T^0 = \tfrac{1}{2}RT \ \ln P_{O_2} \tag{6}$$

where T is the absolute temperature and R the gas constant. Only if the partial pressure of oxygen in the ambient air is higher than the P_{O_2}-value in equation (6) can the oxidation of Ag in ambient air occur. At room temperature (298 K), the equilibrium oxygen partial pressure $P_{O_2} = 1.23 \times 10^{-4}$ atm by inserting $\Delta G^0_{298} = -11.25$ KJ mol^{-1} into equation (6), i.e. only when the oxygen partial pressure is larger than 1.23×10^{-4} atm can the oxidation of Ag occur. In ambient air, the oxygen partial pressure is about 0.2 atm. Therefore, thermodynamically the oxidation of even bulk silver can occur in ambient air at room temperature.

In addition, the curvature of the Ag particle will lead to an increase in the free energy of Ag particles. The increment Δg in the free energy due to the curvature of the Ag particles is given by [20]

$$\Delta g = \frac{2\sigma M}{\rho}\frac{1}{r} \tag{7}$$

where r is the curvature radius of particle, ρ the density, σ the surface energy and M the atomic weight. At room temperature, taking $\sigma = 1400$ erg cm^{-2} [21] and $\rho = 10.5$ g cm^3, we have $\Delta G^0_{298\ \mathrm{K}}(r)$, the standard formation free energy of Ag_2O for the Ag particle with curvature radius r, given by

$$\Delta G^0_{298\ \mathrm{K}}(r) = \Delta G^0_{298\ \mathrm{K}} - 2\ \Delta g = -11.25 - 57.5/r\ \text{(nm) kJ mol}^{-1}.$$

When the particle diameter is 10 nm ($r = 5$ nm), the value of the formation free energy ($|\Delta G^0_{298}(r)|$) will double its value ($\Delta G^0_{298}(r) = -23$ kJ mol^{-1}) and, when the diameter is 3 nm like our sample, the value increases by 3.5 times. Therefore, the driving force of the oxidation for the Ag nanoparticles increases significantly at room temperature, compared with that of bulk silver.

According to the analyses above, we suggest that, when the doped sample is exposed to ambient air at room temperature (298 K), the Ag particles within the pores of silica can undergo physisorption, chemisorption and even oxidation but, in dry air, oxidation is very slow because the endothermic peak for sample 2 is very wide and is caused by the desorption but not decomposition of the oxide. From this, the doped sample, after heat treatment at 623 K for 2 h, was exposed to air with relative humidity greater than 60% at room temperature (298 K) for 1 week. We found that the sample changed from transparent to opaque in 10 h (there is only a small change in transparency for sample 2 during 1 month exposure to dry air) (Ag_2O is also opaque). The corresponding DSC curve, after *in situ* heating at 378 K for 1 h (sample 3.2) is shown in figure 5 (see curve (b)). There is a very high endothermic peak at around 460 K. The sample, after the DSC measurements were finished, was found to be transparent again (an optical study of Ag-particle-doped porous silica will be published elsewhere). The TG curve for this sample is shown in figure 5. There is about 0.92% weight loss in the corresponding temperature region of the endothermic peak.

We know that the decomposition will occur at 467 K [22] for bulk Ag_2O. If the endothermic peak for sample 3 is caused by decomposition of Ag_2O formed during exposure to humid air, the total number N_t of oxygen atoms (O) in the surface layer of the particles can be estimated to be 3.5×10^{20} in 1 g of sample 3.2 according to the weight loss. Hence the Ag–O bond energy of the Ag_2O can be semiquantitatively determined from the ΔH-value of the endothermic peak and the N_t-value (ignoring the difference between enthalpy and internal energy), or $\Delta H/2N_t = 198/2N_t = 1.80$ eV. This bond energy value is larger than the desorption enthalpy of the chemisorbed oxygen (0.9 eV) as indicated above. In addition, the effect of curvature of the particles within the pores will lead to a decrease in the decomposition temperature. Therefore, it is reasonable that the endothermic peak

for sample 3 is attributed to the decomposition of Ag_2O formed by the Ag particles with oxygen during exposure to humid air.

For further verification, the powder consisting of Ag particles of 50 nm diameter, synthesized by the chemical method, was oxidized at room temperature, as described previously [23]. TEM examination shows the coexistence of Ag and Ag_2O. The Ag–Ag_2O powders were measured on the DSC instrument. The DSC curve is shown in figure 8. At 466 K there is a sharp endothermic peak. TEM inspection of the Ag–Ag_2O powder, after DSC measurements, indicates that Ag_2O does not exist. So the sharp peak can be attributed to the decomposition of Ag_2O. As for the exothermic peak at the lower temperature in figure 8, we attribute it to atomic rearrangements at the surfaces of particles [24] and do not discuss it here. Therefore, the endothermic peak at 460 K for sample 3 can also be attributed to the same mechanism, considering that the curvature effect of small size of the particles will lead to a decrease in decomposition temperature.

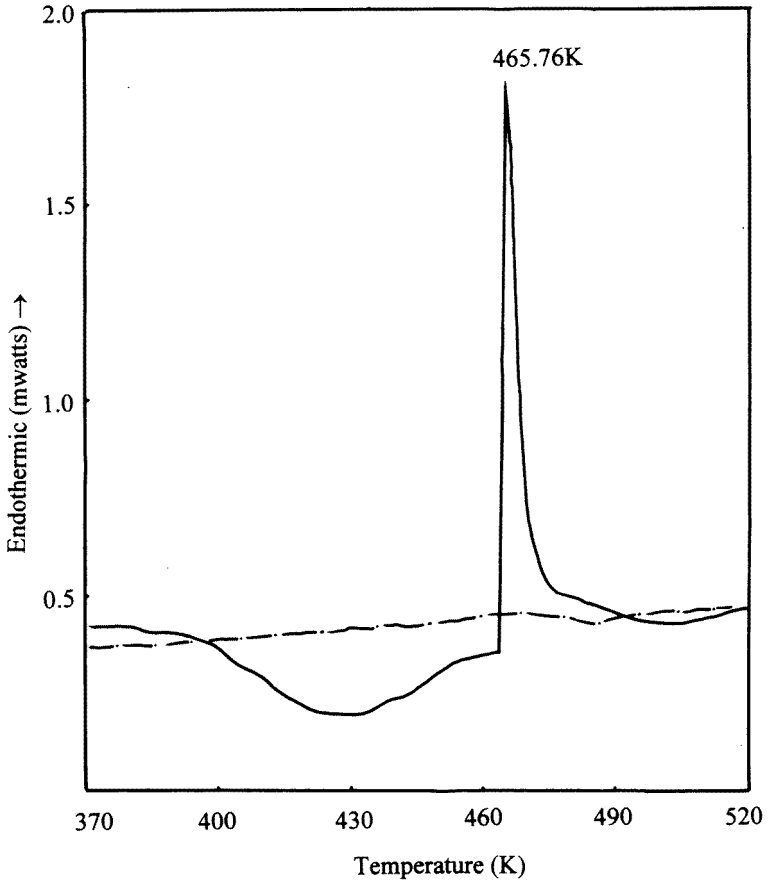

Figure 8. DSC curves for the Ag–Ag_2O powders of 50 nm diameter: — · —, curve obtained in second run.

However, in the TEM diffraction pattern for sample 3, there are no observable diffraction rings of Ag_2O except the Ag rings (the diffraction pattern is the same as in figure 2(b)).

According to the structures and lattice parameters [25] of Ag and Ag_2O, the molar volume V_{Ag} for Ag is 10.3 cm^3 mol^{-1} and V_{Ag_2O} for Ag_2O is 32.2 cm^3 mol^{-1}. Hence, the ratio $V_{Ag_2O}/2V_{Ag} = 1.56 > 1$. This means that the Ag_2O film formed on the surface of Ag particles is dense and is an obstacle to further oxidation. From the N_t-value and the number of surface Ag atoms (3.54×10^{20}) obtained above, the thickness of oxide film on the particle surface can be estimated to be only about two to three atomic layers for sample 3. Furthermore, the volume fraction of Ag particles in the sample is only about 2%, and such a thin oxide film will lead to diffusion of the diffraction rings. All these findings would give rise to difficulty in observing the existence of the Ag_2O film from TEM diffraction. In fact, we have also confirmed the existence of the Ag_2O film from XPS and IR measurements which will be reported elsewhere.

5. Conclusions

Porous silica doped with Ag nanoparticles (about 3 nm in diameter) within its pores was prepared by the sol–gel technique and thermal decomposition of $AgNO_3$. The Ag nanoparticles are uniformly dispersed, and the size distribution can be fitted well by the log-normal distribution function.

The thermal effects for all samples were investigated by DSC. The thermal effects were different if the sample had different treatments before DSC measurement. When the doped sample was exposed to dry air for a short time (2 d) at room temperature (298 K), there was an endothermic peak at around 400 K. However, long exposure to dry air (1 month) resulted in a wider and higher endothermic peak at around 450 K. The origins of both peaks were attributed to the desorption of oxygen physisorbed and chemisorbed, respectively, on the surface of the Ag nanoparticles within the pores. The desorption enthalpy is about 0.26 eV for the lower-temperature peak and 0.90 eV for the other peak.

When the doped sample was exposed to ambient air with relative humidity greater than 60% for 7 d, a much higher endothermic peak exists at around 460 K. This high endothermic peak is attributed to the decomposition of the Ag_2O film formed on the surface of the Ag particles during exposure to the humid air. The Ag–O bond energy in the oxide film is about 1.8 eV.

Because the pores in silica are interconnected and open to ambient air, the Ag particles within the pores are also in contact with the ambient air, which leads to the interaction between the particles and the ambient air. When the doped sample is exposed to ambient air the Ag particles within the pores will first experience physisorption and then chemisorption of the oxygen and finally they will from an oxide film in their surface layer. In humid air, the oxidation process is faster.

References

[1] Kuczynski J and Thomas J K 1985 *J. Phys. Chem.* **89** 2720
[2] Coffer J L, Beauchamp G and Zerda T W 1992 *J. Non-Cryst. Solids* **142** 208
[3] Tanahashi I and Mitsuyu T 1995 *J. Non-Cryst. Solids* **181** 77
[4] Chun-Guey Wu and Thomas B 1994 *Science* **264** 1758
[5] Rao S, Karaguleff C, Gabel A, Fortenbery R, Seaton C and Stegeman G 1985 *Appl. Phys. Lett.* **46** 801
[6] Komiyama H, Hayashi A and Inoue H 1985 *Japan. J. Appl. Phys.* **24** L269
[7] Yasuda T, Komiyama H and Tanaka K 1987 *Japan. J. Appl. Phys.* **26** 818
[8] Halperin W P 1986 *Rev. Mod. Phys.* **58** 533
[9] Suryanarayana C 1995 *Int. Mater. Rev.* **40** 41
[10] Murakata T, Sato S, Ohgawara T, Natanabe T and Suzuki T 1992 *J. Mater Sci.* **27** 1567

[11] Sato S, Murakata T, Suzuki T and Ohgawara T 1990 *J. Mater Sci.* **25** 4880
[12] Weast R C 1989–90 *CRC Handbook of Chemistry and Physics* 70th edn (Raton, FL: CRC) B128
[13] Aller T 1981 *Particle Size Measurement* 3rd edn (London: Chapman & Hall) p 130
[14] Prutton M 1983 *Surface Physics* (Oxford: Clarendon) ch 6
[15] Benard J 1983 *Adsorption on Metal Surfaces (Stud. Surf. Sci. Catal. 13)* (New York: Elsevier) ch 5
[16] Kilty P A and Sachtler W M 1974 *Catal. Rev.* **10** 1
[17] Yoshida S, Murakami T and Tarama K 1973 *Bull. Inst. Chem. Res. Kyoto Univ.* **51** 195
[18] Brandes E A 1983 *Smithells Metals Reference Book* 6th edn (London: Butterworth) pp 8–25
[19] Sonntag R E and Van Wylen G J 1982 *Introduction to Thermodynamics (Classical and Statistical)* 2nd edn (New York: Wiley) p 518
[20] Verhoeven J D 1975 *Fundamentals of Physical Metallurgy* (New York: Wiley) p 169
[21] Verhoeven J D 1975 *Fundamentals of Physical Metallurgy* (New York: Wiley) p 202
[22] Weast R C 1989–90 *CRC Handbook of Chemistry and Physics* 70th edn (Boca Raton, FL: CRC) D46
[23] Uchikoshi T 1989 *J. Japan Inst. Met.* **3** 614
[24] Yong Zhu and Ming Tan 1995 *Mater. Sci. Eng.* A **201** L1
[25] Brandes E A 1983 *Smithells Metals Reference Book* 6th edn (London: Butterworth) pp 6–9